LUMEN SEGMENTATION OF ATHEROSCLEROTIC CAROTID ARTERIES IN CTA

Hui Tang[⋆†] *Theo van Walsum*[⋆] *Reinhard Hameeteman*[⋆] *Michiel Schaap*[⋆]
Aad van der Lugt[⋆] *Lucas J. van Vliet* [†] *Wiro J. Niessen*[⋆†]

[⋆] Biomedical Imaging Group Rotterdam, Departments of Radiology & Medical Informatics,
Erasmus MC, P.O. Box 2040, 3000 CA Rotterdam, The Netherlands
[†]Department of Imaging Science & Technology, Faculty of Applied Sciences,
Delft University of Technology, The Netherlands

ABSTRACT

Lumen segmentation is relevant for quantification of the degree of stenoses and as preprocessing step for the analysis of the vessel wall, and for the simulation and planing of interventions. Although lumen segmentation in CTA has received considerable interest, it remains a challenge for atherosclerotic vessels. In this paper we propose a semi-automatic lumen segmentation method using a levelset approach, which utilizes both boundary information and regional intensity information to accurately segment the lumen of atherosclerotic vessels. The method was trained and evaluated on a publicly available database of 56 carotid arteries. The average Dice similarity coefficient was 88.9 %, the mean absolute surface distance was 0.31 mm. Compared to using only boundary information, this method yields better segmentation in severely atheroslerotic vessels.

Index Terms— lumen segmentation, geodesic active contour, gradient, plaque, calcification, regional information

1. INTRODUCTION

Atherosclerosis is a major vascular disease but asymptomatic in its early stage [1]. Several studies were performed to investigate the relation between atherosclerosis progression and plaque composition [2, 3] or vessel geometry [4]. In these studies, accurate lumen segmentation of atherosclerotic vessels is required for determining vessel geometry or for getting a region of interest for plaque composition analysis. Compared to lumen segmentation in healthy vessels, lumen segmentation in atherosclerotic vessels is more challenging due to the presence of stenoses and plaques.

Computed Tomography Angiography(CTA) is an invasive imaging modality which allows high resolution lumen visualization. The aim of this paper is to develop and evaluate a method that accurately segments the carotid lumen of atherosclerotic vessels in CTA in the presence of plaques.

Geometric deformable models, which are widely used in lumen segmentation [5] for diseased and healthy arteries, include models that use boundary information [6], models that assume a piecewise constant intensity [7] or smooth intensity [8], as well as models using both boundary and regional information [9]. In atherosclerotic vessels, there is a risk that plaque tissue compositions such as calcifications will be segmented as lumen since plaque and lumen intensities are in the same range and because plaques are located close to the lumen. Calcification removal in lumen segmentation can be performed in a preprocessing step [10, 11], during segmentation [12, 13] and in a postprocessing step [14].

In this paper we propose a geometric deformable model based vessel segmentation method for atherosclerotic arteries. This method utilizes both boundary and regional information to steer the lumen surface evolution. The method is initialized by a centerline automatically extracted between user-defined seed points. We evaluate this method on the datasets of the cls2009 challenge [15].

2. METHOD

The proposed segmentation method consists of two steps: centreline extraction and levelset evolution.

2.1. Centreline Extraction

Centrelines are extracted by a minimum cost path approach between user-supplied seed points [16]. We defined the cost, which is used to compute the minimum cost path, as the inverse of the product of a slice-based medialness term [17] and a term indicating how similar a voxel is to the lumen intensity. A small positive constant is added to prevent singularities. The similarity term is used to prevent centrelines passing through plaques.

The extracted centreline is then iteratively refined by performing the minimum cost path in a curved multi-planar reformatted image stack generated perpendicular to the extracted centreline from the previous iteration. More details of this approach are provided in [16].

2.2. Geodesic Active Contour and Region based Segmentation

A geodesic active contour [6] is commonly used to steer the levelset to the lumen border which is defined by a high gradient. However, for atherosclerotic vessels, the gradient magnitude is not sufficient to fine the border since adjacent calcified regions yield an even higher value of the gradient magnitude. Fig. 1(c) shows an example of the gradient magnitude of a carotid artery in CTA. In this case, the gradient between lumen and soft plaque tissue is less strong than the gradient between calcification and soft plaque tissue. Hence there is a risk that the lumen surface will be steered to the border with the strongest gradient. The result will cover the plaque soft region, shown in Fig. 1(b) and Fig. 1(c).

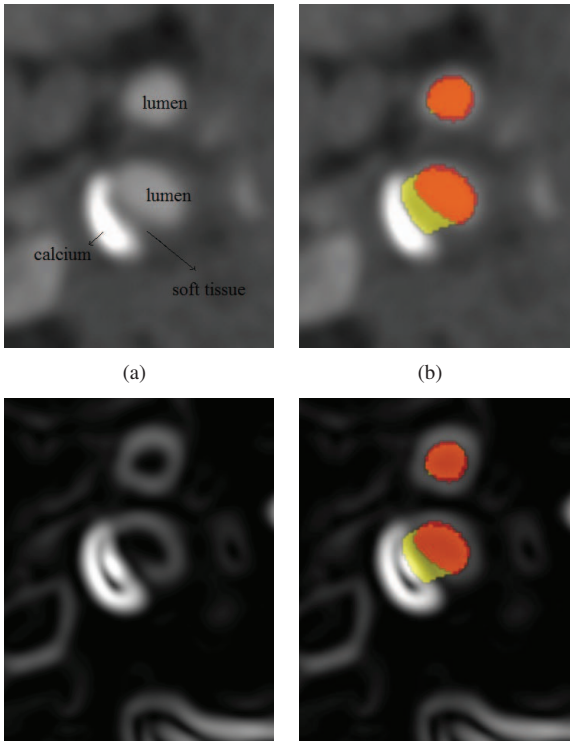


Fig. 1. Example of: (a) original CTA of atherosclerotic carotid arteries (b) original CTA overlayed by manual segmentation (red) and segmentation using only boundary information (yellow) (c) corresponding gradient magnitude (d) corresponding gradient magnitude overlayed by manual segmentation and segmentation using only boundary information.

We therefore include lumen intensity based terms in the energy formulation: the foreground voxels should have an intensity as similar as possible to the lumen intensity and the background voxels should have an intensity as dissimilar as possible to the lumen intensity. Combining this with a geodesic active contour gives the following energy minimization:

$$\begin{aligned} E(\boldsymbol{S}) = \iint_S \gamma P(I(\boldsymbol{S}(u,v)))|\boldsymbol{S}'(u,v)|dudv \\ +\alpha \iiint_{in(\boldsymbol{S})} (1-s(\boldsymbol{x}))dxdydz \\ +\beta \iiint_{out(\boldsymbol{S})} s(\boldsymbol{x})dxdydz \quad , \end{aligned} \tag{1}$$

The parameters α and β are used to weigh the boundary and regional terms. The term $P(I(\boldsymbol{S}))$ is inversely proportional to the gradient magnitude at scale σ_g, $\frac{1}{|G_{\sigma_g} * I|+\eta}$. And $s(\boldsymbol{x})$ determines how similar a voxel is to lumen intensity:

$$s(\boldsymbol{x}) = e^{-(I(\boldsymbol{x})-\bar{I}(\boldsymbol{x}))^2/\sigma^2} \quad . \tag{2}$$

Here $\bar{I}(\boldsymbol{x})$ represents the local mean intensity of the lumen, which is obtained from the closest point on the extracted centreline. Let $\{\boldsymbol{x}_c\}$ denotes the set of points along the centreline, then $\bar{I}(\boldsymbol{x})$ is defined by:

$$\begin{aligned} \bar{I}(\boldsymbol{x}) = I(argmin_{\boldsymbol{x}_c}(d(\boldsymbol{x}-\boldsymbol{x}_c))), \\ \text{subject to:} \quad |\bar{I}(\boldsymbol{x}) - \bar{I}_c| < k\sigma_c \end{aligned} \tag{3}$$

where $\bar{I}_c$ and σ_c are the mean and standard deviation of intensities along the centreline, and $d(\boldsymbol{x}_1, \boldsymbol{x}_2)$ is the Euclidean distance between $\boldsymbol{x}_1$ and $\boldsymbol{x}_2$. k is a constant which controls the tolerance of the constraint. The condition on the difference from the mean intensity prevents outlier intensities along the centreline to be used in the intensity term.

Replacing $\boldsymbol{S}(u,v)$ by $\phi(\boldsymbol{x})$ in Eq. 1, we get

$$\begin{aligned} E(\phi) = \iiint (\gamma H'_\epsilon(\phi(\boldsymbol{x}))P(I(\phi(\boldsymbol{x}))|\nabla\phi(\boldsymbol{x})| \\ +\alpha(1-H_\epsilon(\phi(\boldsymbol{x}))(1-s(\boldsymbol{x}))|\nabla\phi(\boldsymbol{x})| \\ +\beta H_\epsilon(\phi(\boldsymbol{x}))s(\boldsymbol{x})|\nabla\phi(\boldsymbol{x})|)dxdydz \end{aligned} \tag{4}$$

in which $H_\epsilon(\phi(\boldsymbol{x}))$ is a regularized version of the Heaviside function and $H'_\epsilon(\phi(\boldsymbol{x}))$ is its derivative, similar to the approach in [7].

We optimize Eq. 4 by gradient descent:

$$\begin{aligned} \phi_t = H'_\epsilon(\phi(\boldsymbol{x}))\{\gamma \text{div}(P(\phi(\boldsymbol{x}))\frac{\nabla\phi}{|\nabla\phi|}|\nabla\phi| \\ -\alpha(1-s(\boldsymbol{x}))|\nabla\phi| \\ +\beta s(\boldsymbol{x})|\nabla\phi|, \end{aligned} \tag{5}$$

$$\begin{aligned} = H'_\epsilon(\phi(\boldsymbol{x}))\{\gamma\kappa P(I(\phi(\boldsymbol{x})))|\nabla\phi| \\ +\gamma\nabla P(I(\phi(\boldsymbol{x}))) \cdot \nabla\phi \\ -\alpha(1-s(\boldsymbol{x}))|\nabla\phi| \\ +\beta s(\boldsymbol{x})|\nabla\phi|\}. \end{aligned}$$

For tubular structure segmentation, κ is changed to be the minimum curvature [18]. There are four terms in Eq. 5, from top to bottom they are the curvature term, the advection term, the internal regional term, and the external regional term. In our implementation, the curvature term and advection term are weighted separately by γ_c and γ_a instead of γ.

3. EXPERIMENTS

3.1. Data and Implementation

The proposed method is trained on 15 datasets and evaluated on 41 datasets of the "Carotid Lumen Segmentation and Stenosis Grading Challenge". We implemented the proposed method in ITK (*www.itk.org*), ignoring $H'_\epsilon(\phi(\boldsymbol{x}))$ because of the narrow band implementation ($|\phi(x)| < 3$) and the frequent reinitialization.

3.2. Parameter Optimization

We optimized the curvature weight γ_c, the advection weight γ_a and the internal regional weight α by maximizing the dice similarity coefficient (DSC) while fixing the external regional weight β. All other parameters including β are listed in Tab. 1. The curvature weight is varied from 2 to 10 with a step size of 2, the advection weight is varied from 5 to 25 with a step size of 5, the regional weight is varied from 0 to 9 with a step size of 0.01, resulting in 300 combinations. For 15

Table 1. List of fixed parameters.

Parameters	value
minimum RMS error	0.0001
# of iterations	2000
initial tube radius (mm)	2
Gaussian gradient scale (mm)	1
β	1
σ (HU)	90
k	0.5

training datasets, the average DSC is 90.2 %. The optimized parameters are $\gamma_c = 6$, $\gamma_a = 20$ and $\alpha = 0.04$. Fig. 2(a) to Fig. 2(c) show the segmentation accuracy as a function of α and γ_a at different γ_c.

3.3. Results

On 41 carotid arteries of the testing set, the proposed method successfully segmented 38 carotid arteries. Three cases failed due to erroneously extracted centrelines. Tab. 2 and Tab. 3 list our segmentation accuracy. The average DSC is 88.9 %, the average mean surface distance (MSD) is 0.31 mm. Examples of the proposed segmentation method are shown in Fig. 3(a) and Fig. 3(b). We can see that in both cases, the plaque tissue is not included in the segmented lumen.

Table 2. Summary lumen

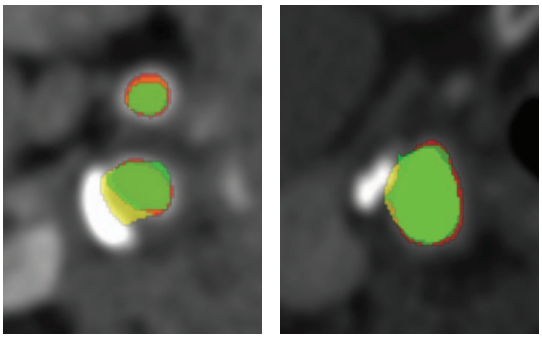
Measure	% / mm		
	min.	max.	avg.
L_dice	72.8%	96.1%	88.9%
L_msd	0.09mm	1.86mm	0.38mm
L_max	0.52mm	10.40mm	2.46mm

Table 3. Averages lumen

Team name	Total success	dice		msd		max		Total rank
		%	rank	mm	rank	mm	rank	
Reference	41	100.0	1.00	0.01	1.00	0.05	1.00	1.00
ObserverA	41	95.1	2.61	0.10	2.68	0.5	2.85	2.72
ObserverB	41	94.6	3.39	0.11	3.37	0.62	2.93	3.23
ObserverC	41	94.4	3.54	0.12	3.34	0.72	3.88	3.59
Gülsün[13]	41	91.8	6.29	0.18	5.78	1.11	5.39	5.82
Krissian[14]	41	87.3	6.41	0.54	7.29	2.98	7.51	7.07
Ours	41	88.9	7.15	0.38	7.80	2.46	7.80	7.59

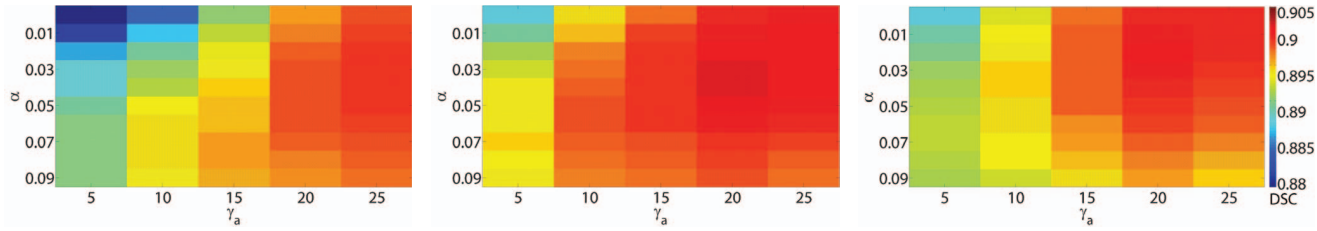
4. DISCUSSION AND CONCLUSION

We presented a semi-automatic levelset based segmentation method for extracting the carotid artery from CTA data. The evolution of the levelset method is steered by both boundary information (gradient magnitude in this study) and internal regional intensity information. Compared to using the gradient magnitude alone, the combined method was better able to delineate the lumen in case of calcified plaques. The weight for each term was optimized by maximizing the DSC between the semi-automatic segmentation and the reference standard. We trained our method on the data of the cls2009 challenge [15]. The proposed method obtained an average Dice similarity coefficent of 88.9 % and an average mean absolute surface distance of 0.31 mm. Our segmentation method performs better than the second place in the challenge on the measures DSC, MSD and max SD, but due to the ranking system, it is ranked third. Upon inspection of the segmentation results, it was observed that sometime the results were not very smooth. Adding a strong smoothing constraint may further improve the results. The presented paper shows that automated segmentation of the carotid artery in CTA has a high potential



(a) (b)

Fig. 3. Segmentation example for an atherosclerotic vessel with optimized parameters, manual (red), geodesic active contour (yellow), geodesic active contour and region (green)



(a) (b) (c)

Fig. 2. Segmentation accuracy as a function of α and γ_a at (a) $\gamma_c = 4$ (b) $\gamma_c = 6$ and (c) $\gamma_c = 8$

to replace manual segmentation for lumen segmentation in atherosclerotic vessels.

5. REFERENCES

[1] Russell Ross, "Atherosclerosis: an inflammatory disease," *New England Journal of Medicine*, vol. 340, pp. 115–126, 1999.

[2] J. M. A. Hofman, et al., "Quantification of atherosclerotic plaque components using in vivo mri and supervised classifiers," *Magn. Reson. Med.*, vol. 55, no. 4, pp. 790–799, 2006.

[3] F Liu, et al., "Automated in vivo segmentation of carotid plaque MRI with morphology-enhanced probability maps," *Magn Reson Med*, vol. 55, no. 3, pp. 659–668, Mar. 2006.

[4] Jonathan B. Thomas, et al., "Variation in the carotid bifurcation geometry of young versus older adults: Implications for geometric risk of atherosclerosis," *Stroke*, vol. 36, no. 11, pp. 2450–2456, Nov. 2005.

[5] David Lesage, et al., "A review of 3D vessel lumen segmentation techniques: Models, features and extraction schemes," *Medical Image Analysis*, vol. 13(6), pp. 819–845, 2009.

[6] V. Caselles, et al., "Geodesic active contours," *International Journal of Computer Vision*, vol. 22(1), pp. 61–79, 1997.

[7] T. F. Chan, et al., "Active contours without edges," *IEEE Transactions on Image Processing*, vol. 10(2), pp. 266–277, 2001.

[8] C. Li, et al., "A level set method for image segmentation in the presence of intensity inhomogeneities with application to MRI," *IEEE Transactions on Image Processing*, vol. accepted, 2010.

[9] Nikos Paragios, et al., "Geodesic active regions and level set methods for supervised texture segmentation," *International Journal of Computer Vision*, vol. 46, no. 3, pp. 223–247, 2002-02-01.

[10] R. Manniesing, et al., "Level set based cerebral vasculature segmentation and diameter quantification in CT angiography," *Medical Image Analysis*, vol. 10, no. 2, pp. 200–214, Apr 2006.

[11] M. Schaap, et al., "Robust shape regression for supervised vessel segmentation and its application to coronary segmentation in CTA," *IEEE Transactions on Medical Imaging*, 2011.

[12] Holger Scherl, et al., "Semi-automatic level-set based segmentation and stenosis quantification of the internal carotid artery in 3d cta data sets," *Medical Image Analysis*, vol. 11, no. 1, pp. 21 – 34, 2007.

[13] M. Akif Gülsün, et al., "Segmentation of carotid arteries by graph-cuts using centerline models," in *Proceeding of Carotid Lumen Segmentation and Stenosis Grading Challenge*, 2009.

[14] Karl Krissian, et al., "A minimal cost path and level set evolution approach for carotid bifurcation segmentation," in *Carotid Lumen Segmentation and Stenosis Grading Challenge, MICCAI 2008 workshop proceedings, 2009*, 2009.

[15] K. Hameeteman, et al., "Evaluation framework for carotid bifurcation lumen segmentation and stenosis grading," *Medical Image Analysis*, vol. In Press, pp. –, 2011.

[16] Hui Tang, et al., "Semiautomatic carotid lumen segmentation for quantification of lumen geometry in multispectral MRI," *Submitted to Medical Image Analysis*.

[17] M. Akif Gülsün, et al., "Robust vessel tree modeling," in *MICCAI*, Berlin, Heidelberg, 2008, MICCAI '08, pp. 602–611, Springer-Verlag.

[18] L. M. Lorigo, et al., "Curves: Curve evolution for vessel segmentation," *Medical Image Analysis*, vol. 5, no. 3, pp. 195–206, Sept. 2001.